Diastereomers of Dibromo-7-*epi*-10-deacetylcephalomannine: Crowded and Cytotoxic Taxanes Exhibit Halogen Bonds

Yi Jiang,[†,‡] Ana A. Alcaraz,[†] Jian-Min Chen,*[,‡] Hisayoshi Kobayashi,[§] Yang J. Lu,[||] and James P. Snyder*[,†]

Department of Chemistry, Emory University, Atlanta, Georgia 30322, Department of Environmental Science and Engineering, Fudan University, Shanghai 200433, China, Institute of Molecular and Cellular Biosciences, The University of Tokyo, Tokyo 113-0032, Japan, and Winship Cancer Institute, Emory University, Atlanta, Georgia 30322

Received September 16, 2005

The diastereomers of dibromo-7-*epi*-10-deacetylcephalomannine (**6** and **7**) have been isolated and characterized. Cytotoxicity and microtubule assembly assays demonstrate that cephalomannine analogue **6** possesses a potency profile very similar to that of Taxol, while isomer **7** is slightly less active. Solid state, solution, and tubulin-bound conformations of the two diastereomers were probed by using X-ray crystallography, 2-D NMR experiments in conjunction with the NAMFIS analysis, and the Glide docking protocol. In the crystal, isomer **7** exhibits an intermolecular halogen bond that may contribute to self-assembly. Neither crystal structure appears in the NAMFIS solution analysis, but both diastereomers are represented in solution by a T-shaped Taxol conformer. Glide docking demonstrates the latter to best fill the tubulin binding pocket, as has been shown for the parent Taxol drug. Each model of the bound complexes for **6** and **7** presents a single well-defined halogen bond from one of the ligand's bromines to Glu22 or Asp26 near the N-terminus of β-tubulin, respectively. This first report of a halogen bond between taxanes and tubulin may prove useful in guiding the design and synthesis of other microtubule-stabilizing agents with a similar capacity.

Introduction

The naturally occurring paclitaxel (Taxol) is a diterpene originally isolated from the bark of *Taxus brevifolia* but now also prepared by semisynthesis and microorganisms.[1,2] The compound is currently regarded as the most promising anticancer agent in the treatment of refractory breast and ovarian cancers.[3−6] It is well-known that paclitaxel exerts its cytotoxic action by binding to microtubules and stabilizing them against depolymerization.[7] An essential structural aspect related to the bioactivity of paclitaxel is the 3-D conformation of the drug, both in solution and bound to its primary tubulin target, the protein that forms microtubules.[8] To date, three models claiming to represent the bioactive form of Taxol in complex with tubulin have received wide attention: the nonpolar,[9−13] polar,[14−16] and T-shaped[17−19] (T-Taxol) conformations. The proposals, based either on 2-D NMR experiments in conjunction with molecular modeling[9−16] or on the electron crystallographic structure of $\alpha\beta$-tubulin stabilized by zinc cations and Taxol,[18,20] were presented in the hope that more efficacious analogues might be designed. Our recent disclosure[19] of a class of highly active bridged taxanes provides both experimental and theoretical evidence that a C4 to ortho-C3′ linkage based on the T-Taxol conformer is one effective means of improving potency. Related studies provide additional support for the T-Taxol template.[21,22] In the present work, we extend conformational considerations to two diastereomers of dibromo-7-*epi*-10-deacetylcephalomannine, whose in vitro cytotoxicities are similar to that of Taxol.[23] Previously, we reported the stereochemical assignments of the two diastereomers based on the crystal structure of one of them.[23] Two further issues taken up here are (1) the possible role played by interatomic interactions involving bromine atoms in both crystal structures and the ligand−tubulin binding complexes, and (2) the relationship between taxane conformation in solution and in the bound tubulin complex.

Extensive surveys of entries in the Cambridge Structural Database[24−26] coupled with ab initio calculations[26] have defined the geometry of halogen bonds in crystal structures. The quantum chemical calculations imply that the interaction is primarily electrostatic, with contributions from polarization, dispersion, and charge transfer components. The stabilizing potential of a halogen bond is estimated to range from about half to slightly greater than that of an average hydrogen bond in directing the self-assembly of organic crystals.[27,28] A recent parallel survey of protein and nucleic acid structures reveals similar noncovalent interactions with potential for stabilizing ligand binding and molecular folding.[29]

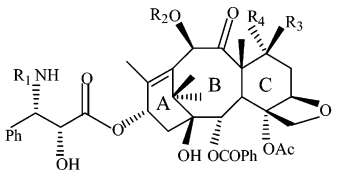

1	R_1=Bz, R_2=Ac, R_3=OH, R_4=H	**Paclitaxel**
2	R_1= Tigloyl, R_2=Ac, R_3=OH, R_4=H	**Cephalomannine**
3	R_1=Boc, R_2=H, R_3=OH, R_4=H	**Docetaxel**
4	R_1=Bz, R_2=H, R_3=H, R_4=OH	**7-*Epi*-10-deacetyltaxol**
5	R_1= Tigloyl, R_2=Ac, R_3=H, R_4=OH	**7-*Epi*-10-deacetylcephalomannine**

In the present study, an investigation of the solid state, solution, and tubulin-bound conformations of the two diastereomers of dibromo-7-*epi*-10-deacetylcephalomannine was undertaken and correlated with biological activities. An important outcome is that a halogen bond is suggested to play an important role in both the assembly of the crystal structure of one of the

* To whom correspondence should be addressed. Phone: 404-727-2415. Fax: 404-727-6586. E-mail: snyder@euch4e.chem.emory.edu (J.P.S.) or jmchen@fudan.edu.cn (J.-M.C.).
[†] Department of Chemistry, Emory University.
[‡] Fudan University.
[§] University of Tokyo.
[||] Winship Cancer Institute, Emory University.

10.1021/jm0509243 CCC: $33.50
Published on Web 02/16/2006

Scheme 1. Synthesis of Compounds **6** and **7**

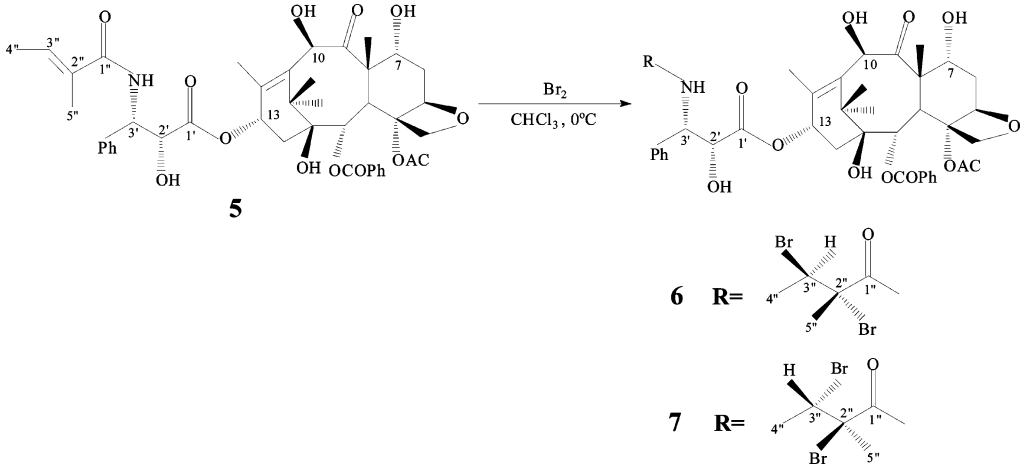

isomers (**7**) and the enhancement of the tubulin binding affinity of the other (**6**). In addition, we have performed NAMFIS analyses and tubulin-docking studies for both isomers to obtain conformational populations in solution and to evaluate possible bioactive forms, respectively. The result that the T-Taxol conformer is present in solution and simultaneously predicted to be the favored bound entity reinforces previous reports from this laboratory proposing a connection between solution and ligand-bound structures.

Synthesis and Characterization of Diastereomers 6 and 7. The diastereomers **6** and **7** were synthesized by treating crude plant extract containing 7-*epi*-10-deacetylcephalomannine in cooled chloroform with bromine (Scheme 1). Isolation of the two diastereomers was accomplished by normal-phase and reverse-phase preparative chromatography in turn to obtain analytically pure samples. The two brominated cephalomannine derivatives were characterized by NMR and APCI MS (see Experimental Section).

If, as expected, a stereoselective anti-addition mechanism is operating,[30] the two products obtained by bromination of **5** must differ in the stereochemistry at C2″ and C3″. Although brominated derivatives of cephalomanine and 7-*epi*-cephalomannine have been synthesized by others and shown to exhibit strong cytotoxicities,[31,32] the stereochemical assignments of these compounds have not been established. This may have presented an obstacle for further development of these potentially valuable bioactive compounds.

Compared with the ^{1}H NMR spectrum of **5**, two major differences appear in the corresponding spectra of **6** and **7**: (a) an upfield shift of the C3″ proton signal from a quartet at ca. δ 6.43 to a similarly split resonance ca. δ 4.6, and (b) a downfield shift of the C5″ proton signal from a doublet at ca. δ 1.7 to singlets at ca. δ 1.99 and 1.94. The two shifts can be attributed to the altered character of the brominated sp^3 carbon (C3″) and to the bromine atoms' addition at the vicinal C2″ position. Other than a small change in the C5″ proton signals, no diagnostic differences are apparent between the ^{1}H NMR, ^{13}C NMR, H−H COSY, and C−H COSY spectra of **6** and **7** (a full table of ^{13}C NMR chemical shifts is available in the Supporting Information). Consequently, we resort to X-ray crystallography to assign the stereochemistry of the adducts.

Cytotoxicities and Tubulin Polymerization. The cytotoxicities of the two diastereomers along with paclitaxel were evaluated in vitro against three tumor cell lines: MCF-7 (breast), A549 (non-small-cell lung), and A2780 (ovarian) by applying the MTT procedure.[33] In terms of IC$_{50}$, the two diastereomers exhibit similar cytotoxicity against the A2780 and MCF-7 human cancer cell lines as compared to paclitaxel. The compounds are 10-fold weaker as measured by the A549 cell line. In the tubulin polymerization assay, **6** is essentially identical to paclitaxel, while **7** is slightly weaker (Figure 1).

X-ray Crystal Structure Determination. We previously reported that diastereomer **6** crystallizes from acetonitrile in the monoclinic system with space group *C*2 and sustains (2″*S*,3″*R*) stereochemistry.[23] In the present work, compound **7** crystallizes from an acetonitrile−ether mixture in the orthorhombic system with space group *P*2(1)2(1)2(1) and displays (2″*R*,3″*S*) stereochemistry. As shown in Figure 2, the molecular structures of diastereomers **6** and **7** are similar in overall shape with the major difference in conformation appearing at the termini of the C13

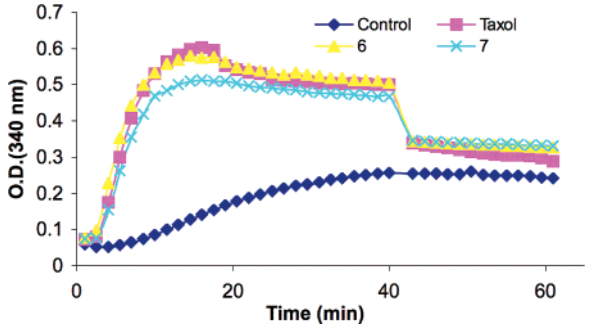

Figure 1. Tubulin polymerization−depolymerization activies of Taxol, **6**, **7** and control.

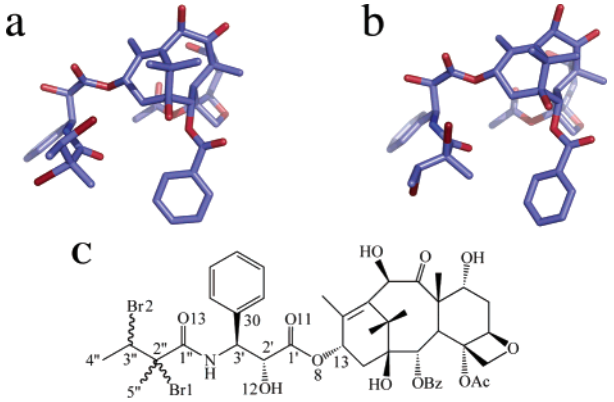

Figure 2. X-ray structures of (a) **6** and (b) **7** and (c) the labeling scheme of selected atoms of the C13 side chains of **6** and **7**. Two water molecules and one acetonitrile molecule in the structure of **7** are omitted for the sake of clarity.

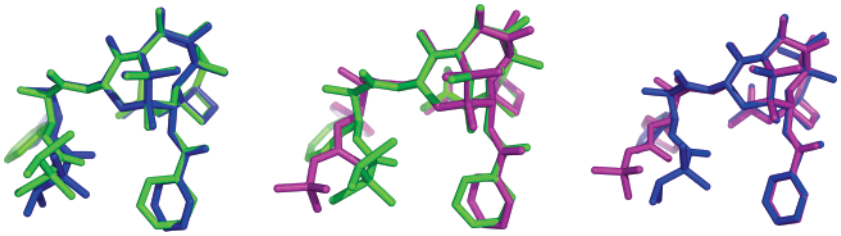

Figure 3. From left to right, comparison of the crystal structures of **6** and **7**, **6** and docetaxel, and **7** and docetaxel by superposition of the tetracyclic baccatin cores; **6** (green), **7** (blue), docetaxel (pink).

Table 1. Selected Torsion Angles (deg) for the C13 Side Chains of **6**, **7**, Conformer A of 7-*epi*-10-Deacetyltaxol, Docetaxel, and T-Taxol

torsion angle[a]	**6**	**7**	7-*epi*-10-deacetyltaxol (A)	docetaxel	T-taxol
C13−O8−C1′−O11	8.9	5.0	11.8	−6.6	0.6
C13−O8−C1′−C2′	−169.4	−176.4	−166.6	168.0	−178.7
O8−C1′−C2′−O12	179.3	171.4	−134.0	−176.7	178.1
O8−C1′−C2′−C3′	56.2	48.6	108.3	60.2	55.7
O11−X1′−C2′−O12	1.0	−10.0	47.5	−2.2	−1.2
O11−C1′−C2′−C3	−122.1	−132.8	−70.0	−125.3	−123.7
C1′−C2′−C3′−C30	178.3	−175.3	−66.0	−179.4	178.0
C1′−C2′−C3′−N1	53.4	57.0	168.8	56.4	52.4
H2′−C2′−C3′−H3′	56.5	60.8	64.2	57.3	55.4
O12−X2′−C3′−N1	−68.7	−66.3	51.7	−64.7	−67.0
O12−C2′−C3′−C30	56.2	61.4	176.4	59.5	58.5
C2′−C3′−N1−C1″	−138.0	−131.3	−143.0	−141.3	−153.4
H3′−C3′−N1−H1A(N1)	157.7	163.9	153.6	159.4	147.3
C30−C3′−N1−C1″	95.9	101.2	92.4	97.3	82.8
C3′−N1−C1″−O13	6.1	−0.2	−3.0	12.8	−1.0

[a] See Figure 2c for atom labeling of **6** and **7**.

side chains. This results in a different orientation of the two bromine atoms at C2″ and C3″ in the two compounds. The core tetracyclic ring systems of both diastereomers are rigid and present as essentially identical by comparison with all other baccatin derivatives resolved by X-ray analysis.[34−37]

Throughout the history of taxane synthesis and biological evaluation, molecular conformation has been related to bioactivity.[38,39] Three extremes have been discussed most frequently in terms of the spatial disposition of the C13 side chains, i.e., the nonpolar,[9−13] polar,[14−16] and T-shaped conformations.[17−19] Interestingly, the former two conformers have also been observed in crystal structures of paclitaxel[34] and its two active analogues, 7-*epi*-10-deacetyltaxol[35] and docetaxel.[36] The T-Taxol form was recognized in the deconvolution of the average spectra of paclitaxel in chloroform[17] and was subsequently proposed to be the bound conformation on β-tubulin.[18] Recent experimental evidence from highly active constrained Taxol analogues is strongly supportive that the T-Taxol conformation represents the essential features of taxane binding to microtubules.[19]

As revealed by Figure 3, the C13 side chains of **6** and **7** in the solid state are in folded conformations. Consequently, the C3′ dibrominated tigloyl moieties (C1″ to C5″) are directed toward the C2 benzoate groups, while the C3′ phenyl rings are projected away from the taxane cores. This orientation is reminiscent of the nonpolar conformer[9−13] and the crystal structure of docetaxel[36] but in contrast to the polar form observed in the crystal structures of paclitaxel[34] and analogues.[35] For more detailed comparison of C13 side chain conformations, Table 1 lists selected torsion angles for **6**, **7**, docetaxel, 7-*epi*-10-deacetyltaxol, and T-Taxol. As suggested by the torsion angles of the two diastereomers and the polar conformation represented by conformer A of 7-*epi*-10-deacetyltaxol, the variations in torsion angles around the C1′−C2′ and C2′−C3′ bonds seem to dominate changes in the orientation of the side chain relative to the core. For **6**, **7**, docetaxel, and T-Taxol, these differences are small and reflect a common conformation along the C1′ to C3′ chain of atoms. Despite the great similarity between the C13 side chain dihedral angles of **6** and **7**, the placement of the brominated tigloyl group is somewhat different between the two diastereomers. The bulky bromine atoms cause small differences of 5°−7° in the dihedral angles along the C1′ to C2″ chain of atoms, resulting in a kind of lever effect at the tigloyl termini.

Another striking difference concerns interatomic interactions. The distances between two protons of the C5″ methyl group (H 5″A and H 5″C) and the ortho- and meta-protons of the C2 benzoyl phenyl ring are 3.6, 2.8 Å and 3.3, 3.2 Å in **6** and **7**, respectively. Thus, the C5″ methyl groups are in weak van der Waals contact with the C2 benzoyl phenyl rings in both diastereomers. No such hydrophobic interactions are observed between the corresponding moieties in T-Taxol, reinforcing the notion that small changes in a single dihedral angle can have a decisive impact on molecular conformation. Furthermore, by comparison with the shortest H···H distance from the methyl groups of the *tert*-butyl group to the C2 benzoyl phenyl rings in docetaxel (3.7 Å), it is apparent that the hydrophobic side chain−side chain interactions in the diastereomers are much more pronounced.

It is interesting to note that although the C3′ phenyl rings project away from the taxane ring core in the diastereomers, the shortest separations between protons of these rings and the C4 acetyl methyl groups are 3.0 and 2.7 Å in **6** and **7**, respectively. These distances are much shorter than the corresponding ones in the crystal structure of 7-*epi*-10-deacetyltaxol [3.9 (A) and 4.0 Å (B)][35] but similar to those in the X-ray structures of paclitaxel [3.4 (A) and 2.7 Å (B)][34] and docetaxel (2.7 Å).[36] Although the same C4/C3′ collapse in T-Taxol (2.3 Å)[17] motivated the synthesis of highly active tethered taxanes,[19] the earlier structures did not do so. This is undoubtedly because all of them represented either polar or nonpolar conformations in which one of the C13 terminal hydrophobes (Ph or *t*-Bu) was clustered with the terminal phenyl of the C2 side chain. Accordingly, these larger groups were regarded as the appropri-

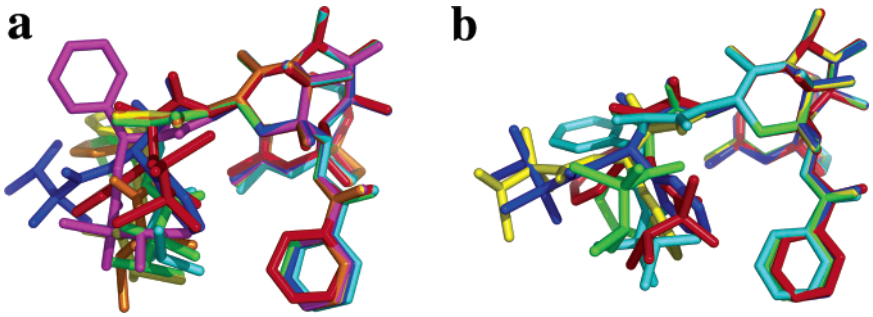

Figure 4. Baccatin superposition of structures of dibromo diastereomers **6** and **7**: (a) **6** and six of its NAMFIS conformations in red (**6**), blue, green, pink, orange, cyan, and yellow, respectively, and (b) **7** and four of its NAMFIS conformations in red (**7**), blue, yellow, cyan, and green, respectively.

ate centers for synthetic manipulation and subsequent tethering. Unfortunately, few of them proved to show Taxol-like activity.[39]

In both crystal structures of the two diastereomers, intra- and intermolecular hydrogen bonds are observed, with all hydroxyl groups engaged in hydrogen bonds. Two water molecules and one acetonitrile molecule reside in each asymmetric unit of crystal structure of **7**, while no solvent molecules are observed in the solid-state lattice of **6**. The presence of solvent molecules is certainly responsible for the different distribution of hydrogen bonds in the two diastereomers. In compound **6**, the folded conformation is stabilized by four intramolecular hydrogen bonds between the O12 hydroxyl and the C3′ amide nitrogen [*r*(O···N) 2.9 Å], the O1 hydroxyl and O9 [*r*(O···O) 3.2 Å], the O5 hydroxyl and O10 [*r*(O···O) 2.9 Å], and the O7 hydroxyl and O6 [*r*(O···O) 2.7 Å]. In addition, one nonconventional hydrogen bond involving one of the two bromine atoms is observed in **6** ($CH14_B$···Br2, 2.9 Å), a special contact between side chain and baccatin core that might be partially responsible for the crowded structure. The solid-state molecular packing in **6** is due to a combination of van der Waals interactions as well as intermolecular H-bonds. The latter encompass noncovalent interactions between the hydroxyls at carbons 1, 7, and 12 and the amide group in one molecule and O4, O6, O9 atoms in the adjacent molecule.

For compound **7**, intramolecular hydrogen bonds are observed between the O5 hydroxyl and O10 [*r*(O···O) 2.8 Å], the O12 hydroxyl and the C3′ amide nitrogen [*r*(O···N) 2.9 Å], and the O12 hydroxyl and O11 [*r*(O···O) 2.7 Å]. No intramolecular nonconventional hydrogen bonds involving bromine atoms were found for this compound. Likewise in the unit cell of **7**, no direct intermolecular hydrogen bonds are observed between molecules. However, molecules of the dibromide are linked to each other by means of intervening water and acetonitrile solvent molecules. Surprisingly, the only direct interaction between different entitites of **7** is a halogen bond.[40] The Br at C3″ in one molecule is paired with the carbonyl oxygen of the C2 benzoyl group (C3″−Br···O9−C21) in an adjacent structure, resulting in infinite chains along the *b*-axis. Supporting the presence of a genuine halogen bond, and its possible role in self-assembly for **7** during crystal formation, is the distance between C3″−Br and O9 [*r*(Br···O 3.2 Å vs the van der Waals sum[41] 3.37 Å] and the C3″−Br···O angle of 173°.[24−29] Both values conform to the characteristic bond length and angle linearity of the halogen bond resulting from a screen of the Cambridge Structural Database.[25,26] The presence of such an important interaction in the solid state for one of the diastereomers encouraged us to explore the solution and binding conformations of **6** and **7** to learn if halogen bonds might contribute to microtubule binding affinity as well.

Table 2. Populations, $\Delta\Delta G$ (kcal/mol), and ΔE (kcal/mol) for the Conformers of Both **6** and **7** Derived from NAMFIS Analysis in DMSO-d_6/D_2O and MMFF/GBSA/H_2O MMFF, Respectively

6	pop. (%)	$\Delta\Delta G$	ΔE	family	**7**	pop. (%)	$\Delta\Delta G$	ΔE	family
I	49	0.0	6.6	polar	**I**	45	0.0	5.6	nonpolar
II	27	0.4	6.2	T-form	**II**	26	0.3	5.4	polar
III	7	1.2	6.6	nonpolar	**III**	25	0.4	5.3	polar
IV	6	1.3	6.1	nonpolar	**IV**	4	1.5	2.2	T-form
V	6	1.3	4.9	nonpolar					
VI	5	1.4	6.5	T-form					

NAMFIS Analysis for 6 and 7. NAMFIS (*N*MR *a*nalysis of *m*olecular *f*lexibility *i*n *s*olution) is a method that combines quantitative 2-D NOE determination with extensive conformational analysis to deconvolute an averaged ^{1}H NMR into an estimate of specific mole fractions for the contributing and rapidly equilibration conformations.[42,43] In the present cases, 33 and 31 intramolecular distances for **6** and **7**, respectively, were derived by 2D ROESY NMR analysis and fitted with 3251 and 2548 fully optimized MMFF/GBSA/H_2O conformations, respectively (See Experimental Section and Supporting Information).

NAMFIS analysis for **6** resulted in six conformations ranging in population from 49% to 5% with a sum of square differences (SSD[42,43]) of 27% (Figure 4a, Table 2). Similarly, the analysis for **7** delivered four conformers ranging in population from 45% and 4% with an SSD of 9 (Figure 4b, Table 2). The NAMFIS conformers of **6** (**I**−**VI**) and **7** (**I**−**IV**) can be conveniently placed in three broad families. Structure **6-I**, the dominant conformation (49%), adopts the polar motif exhibiting C2 to C3′ phenyl−phenyl hydrophobic collapse. The second subset includes **6-II** and **6-VI** with populations of 26% and 5%, respectively. Like T-Taxol, these conformers are open, placing their C3′ phenyl rings distant from the C2 phenyl. Of the two, conformer **6-II** most closely resembles T-Taxol. Conformers **6-III** and **6-IV** (7% and 6%, respectively) correspond to the nonpolar motif, displaying collapse between benzamido phenyl groups and the C2 Ph.

The most highly populated NAMFIS solution structure for compound **7** (**7-I**, 45%), unlike **6**, is a nonpolar conformer. The next pair with equal populations, **7-II** and **7-III** (25 and 26%, respectively) are polar forms that display C2 to C3′ phenyl−phenyl clustering. Conformer **7-IV** with the lowest population (4%) is a T-Taxol family member. This result is reminiscent of the situation of Taxol itself. In both polar and nopolar solvents, the T-form appears with a population below 5%.[17]

The NAMFIS results for diastereomers **6** and **7** are noteworthy in two respects. First, the dibromo compounds yield 30−50% fewer conformations than Taxol itself.[17] This is most likely

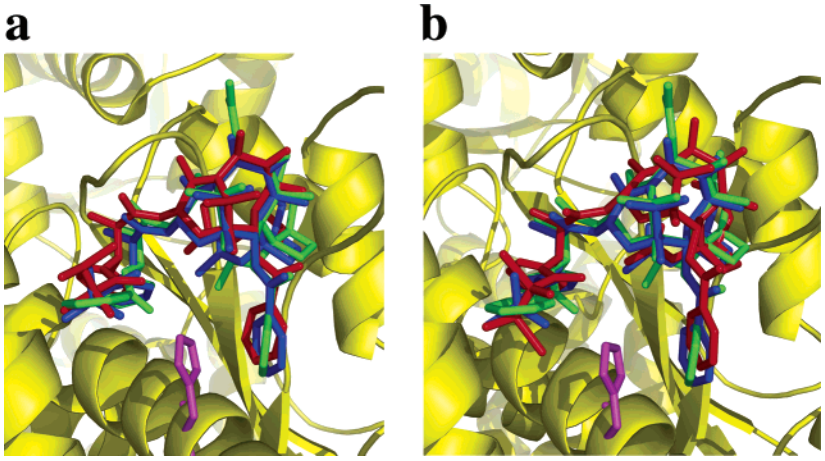

Figure 5. Docking poses of Taxol (green), Taxotere (blue), and the brominated diastereomers (red) within the taxane−tubulin binding pocket: (a) **6** and (b) **7**.

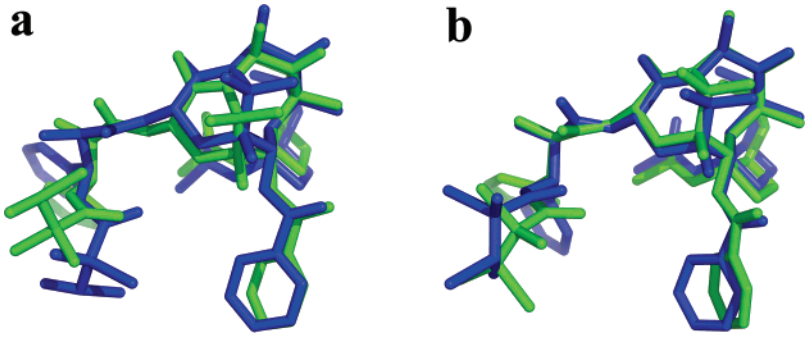

Figure 6. Superposition of the NAMFIS T-Taxol conformers and the docking poses of (a) **6-II** (blue) and the model of bound **6** (green) and (b) **7-IV** (blue) and the model of bound **7** (green).

a result of steric crowding caused by the two bulky bromine atoms leading to fewer low-energy conformations. Second, as shown in Figure 4, the X-ray crystal structures for neither diastereomer are found in the NAMFIS conformational pool. This result was obtained although the conformational databases were enriched with the original X-ray structures of **6** and **7** prior to conformer deconvolution. Their MMFF/GBSA/H_2O energies range from 4.9 to 6.6 and 2.2 to 5.6 kcal/mol from the global minima (not observed among the NAMFIS conformers) as determined by conformational searches performed with MMFF.

Conformer Energies; $\Delta\Delta G$ vs ΔE. If the conformer populations as derived by NAMFIS are accurate or reasonably so, then the Boltzmann equation permits an evaluation of conformer energies relative to the global minima of **6-I** and **7-I**. The corresponding values are recorded in column 3 of Table 2. Since the populations represent a given state in an experimental setting, they are free energy differences ($\Delta\Delta G$) that apply to the context of the NMR measurements; i.e. in DMSO-d_6/D_2O at ca. 30 °C. Relative to the experimental global minimum, the free energy window ranges from 0 to 1.5 kcal/mol. This evaluation contrasts sharply with the relative energies predicted by the MMFF/GBSA/H_2O force field (column 4, Table 2) in two significant respects. First, relative to the MMFF global minima, the energies range across a wider window: 2−6.6 kcal/mol. Second, the lower population conformers are associated with the lower energies. As pointed out previously,[44] force field energies can be notoriously capricious when they are applied to highly polar, complex, and polyfunctional molecules in solution, e.g. taxanes. It would seem that the MMFF/GBSA/H_2O predicted energies for **6** and **7** are no exception.

Docking Diastereomers 6 and 7 into Tubulin. The NAMFIS conformers **6-II** and **7-IV** (Table 2) with the closest likeness to that of T-Taxol were separately and flexibly docked into the β-tubulin pocket by using the Glide docking program.[45] As shown in Figure 5, the corresponding binding conformations for both isomers fit the pocket nicely and overlap well both the baccatin core and the three terminal phenyl rings of tubulin-bound T-Taxol in a slight modification of the refined electron crystallographic complex.[20]

The various functional groups in the two diastereomers and in Taxol enjoy similar interactions with the protein binding site, including a number of key hydrophobic interactions and hydrogen bonds. Both ligand models are likewise remarkably similar to their NAMFIS DMSO-d_6/D_2O counterparts (Figure 6). Indeed, NAMFIS solution conformers for Taxol and epothilone A were employed as docking templates as part of the refinement process for determining the corresponding bioactive β-tubulin-bound conformations.[18,46] In both cases, low-population conformations were a key to structure determination. We assume this strategy finds a parallel in the present analysis. Thus, the similarity of the tubulin binding poses and the tubulin polymerization capacities among the three compounds is entirely consistent with the proposition that not only Taxol but also the brominated cephalomannines adopt the T-form upon binding to tubulin.

Structurally, the termini of the C13 side chains of **6** and **7** resemble more that of the nonaromatic Taxotere rather than that of Taxol. Therefore, to make a full comparison, Figure 5 also depicts the docking of Taxotere into the tubulin pocket by means of the Glide procedure. Instead of van der Waals-mediated π-ring contacts between Taxol's C3′ benzamidophenyl center and the His229 imidazole ring in tubulin, one of Taxotere's *t*-Bu methyl groups plays the same role in its nonbonded encounter with the imidazole, a phenomenon previously ob-

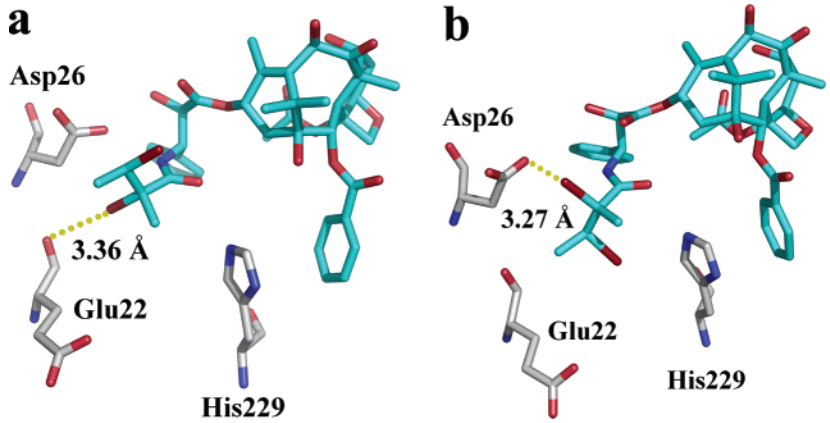

Figure 7. The disposition of halogen bonds for diastereomers within the tubulin−ligand binding complex: (a) **6** and Glu22 and (b) **7** and Asp26.

served by means of alternative docking procedures.[47,48] Likewise, a van der Waals interaction between the C5″ methyl group in **6** and the His229 imidazole is obtained. While neither of the methyl groups in the C3′ terminal tiglolyl groups in **7** are within van der Waals distance of the His229 imidazole, the C4″ methyl group of **7** does make van der Waals contact with the protein's Glu22 in the docked complex.

Potential Taxane−Tubulin Halogen Bonds. In a previous section, we pointed out that the crystal lattice of diastereomer **7** incorporates a halogen bond that possibly contributes to its assembly during crystallization. A recent survey of protein and nucleic acid structures reveals that similar halogen bonds may well provide stabilizing inter- and intramolecular interactions affecting ligand binding and molecular folding.[29] The geometry required for the formation of such the bonds was defined as (i) the distance between halogen atom and oxygen atom being less than or equal to the sum of respective van der Waal radii (3.37 Å for Br···O) and (ii) a C−X···O angle ≈165° and an X−O···Y angle ≈120°. In the model ligand−tubulin complex of **6** (Figure 7a), an association between Br1 and an oxygen atom from Glu22 conforms to the required geometry [*r*(Br---O) 3.36 Å, *θ*(C−Br···O) 169°, *θ*(Br−O···C) 106°].

Halogen bonds are stabilized to an extent of 2−3 kcal/mol, making them energetically equivalent to C−H···O or C−H···N hydrogen bonds.[26] Therefore, in **6** it is not unreasonable to suppose that the hydrophobic interactions between the C5″ methyl group and the His229 imidazole combined with the putative halogen bond contribute sufficiently to promote tubulin polymerization equivalent to that of Taxol.

In the binding complex of **7**, there is also a close contact between Br at C2″ and an oxygen atom from the Asp26 residue (Figure 7b). The Br···O distance is below the van der Waals sum at 3.27 Å, while the C−Br···O and Br···O═C angles are less ideal at 139° and 70°, respectively. On one hand, although this modeled contact in **7** cannot be defined rigorously as a halogen bond, we believe the short separation between the Br and O atoms may still lead to a moderate electrostatic interaction that adds to other forces responsible for the binding affinity of **7**. On the other hand, absence of an intermolecular hydrophobic contact between the C5″ methyl group and His229 may be the factor behind the slightly weaker capacity to promote tubulin polymerization to microtubules.

Summary and Conclusions

The diastereomers of dibromo-7-*epi*-10-deacetylcephalomannine (**6** and **7**), previously shown to be nearly as cytotoxic as paclitaxel, are also potent stabilizers of microtubules. Given the compounds' direct action on the protein and the potential for the bromines at C2″ and C3″ to introduce severe steric crowding on the highly critical taxane C13 side chain, we subjected the compounds to structural and conformational analysis in the solid state, in solution, and in complex with tubulin. In the solid state, **6** and **7** display nonpolar conformers similar to that of docetaxel (Figure 2) and anticipate conversion to the T-form (Figures 5 and 6) with minimal torsional reorganization. In the crystal lattice, diastereomer **7** possesses the novelty of a halogen bond. The Br at C3″ in one molecule is paired with the C═O oxygen of the C2 benzoyl group (C−Br···O═C) in an adjacent structure. While water and acetonitrile solvent molecules coupled to the taxane in the crystal lattice serve to produce infinite chains along the *b*-axis, the short Br···O distance (3.17 Å) and the ideal halogen bond angle (C−Br···O, 173°) suggest that the halogen bond is a primary contributor to both lattice structure and self-assembly.

NAMFIS deconvolution of the conformers of **6** and **7** in 80% DMSO-d_6/20% D_2O resulted in fewer solution conformations by comparison with paclitaxel, most likely a result of steric crowding. Nonetheless, the T-taxane form is represented in both sets of isomers (Figure 6) similar to the situation for the Taxol parent.[17] And like T-Taxol, these structures are predicted to bind to β-tubulin in the same manner (Figure 5). As a complement to bonding forces observed in the crystal for **7**, the Glide-docked tubulin ligand complex of **6** exhibits an ideal Br···O (Glu22) halogen bond (Figure 7). Isomer **7** is similarly situated with respect to Asp26, but the bond angles around bromine are not optimal (Figure 7). Nevertheless, certainly **6** and perhaps **7** would seem to benefit from the halogen bond association with the protein, a unique observation for taxane−tubulin binding. The potential roles played by halogen in the dibromo-7-*epi*-10-deacetylcephalomannines studied here suggest novel design possibilities for other microtubule-stabilizing compounds as well.

Experimental Section

Synthesis of Dibromo-7-*epi*-10-deacetylcephalomannine Diastereomers 6 and 7. Crude plant extract (3.0 g) containing 14.8% paclitaxel, 16.1% cephalomannine, 24.7% 7-*epi*-10-deacetylcephalomannine, and 38.5% 7-*epi*-10-deacetylpaclitaxel was dissolved in chloroform so that a total of 250 mL of solution was obtained. To this solution, cooled in an ice bath and continually stirred with a magnetic stirrer, was added chloroform (30 mL). To the cooled solution (0 °C), bromine (100 μL) was added dropwise. After 30 min of reaction in the dark, the reaction mixture was then washed with 30 mL of 5% aqueous sodium sulfite solution, followed by two washes with distilled water (2 × 20 mL). The combined aqueous layer was then reextracted with chloroform (30 mL). The organic layers were combined, dried with anhydrous sodium sulfate (10 g), and evaporated to dryness using a rotary vacuum evaporator

at 30 °C. The resulting brominated material was purified by preparative HPLC [mobile phase ethyl acetate/*n*-hexane (1:1)] followed by reverse phase preparative HPLC [mobile phase acetonitrile/water (40:60)] to yield high-purity **6** (0.25 g) and **7** (0.24 g) as light yellow and white powders, respectively.

Compound 6: mp 171−173 °C; UV λ_{max} MeOH (ϵ) 195 nm; ^{1}H NMR ($CDCl_3$) δ 1.09 (s, 3H), 1.24 (s, 3H), 1.72 (s, 3H), 1.74 (m, 3H), 1.75 (s, 3H), 1.99 (s, 3H), 2.29 (m, 2H), 2.32 (m, 2H), 2.44 (s, 3H), 3.68 (dd, J = 2.27, 2.35, ^{1}H), 3.91 (d, J = 7.37, 1H), 4.39 (t, J = 9.39, 2H), 4.60 (q, 1H), 4.71 (d, 1H), 4.90 (dd, J = 3.92, 3.76, 1H), 5.42 (s, 1H), 5.56 (dd, J = 1.76, 1.95, 1H), 5.73 (d, J = 7.37, 1H), 6.22 (t, J = 8.45, 1H), 7.36−8.12 (m, 11H); ^{13}C NMR ($CDCl_3$) δ 14.3, 16.7, 20.5, 22.5, 22.6, 26.0, 26.7, 35.3, 36.3, 40.2, 42.5, 54.3, 55.2, 57.3, 72.7, 72.8, 75.5, 75.8, 76.7, 77.0, 77.2, 79.2, 82.1, 82.6, 126.5, 128.3, 128.7, 129.0, 129.3, 130.1, 133.7, 135.8, 137.3, 137.7, 167.0, 168.7, 172.2, 172.3, 214.9; APCI full MS m/z $[M + Na]^+$ 971.58.

Compound 7: mp 176−178 °C, UV λ_{max} MeOH (ϵ) 196 nm; ^{1}H NMR ($CDCl_3$) δ 1.09 (s, 3H), 1.23 (s, 3H), 1.72 (s, 3H), 1.73 (m, 3H), 1.74 (s, 3H), 1.94 (s, 3H), 2.29 (m, 2H), 2.31 (m, 2H), 2.46 (s, 3H), 3.68 (dd, J = 2.18, 2.60, 1H), 3.91 (d, J = 7.30, 1H), 4.39 (t, J = 8.93, 2H), 4.60 (q, 1H), 4.72 (d, 1H), 4.89 (dd, J = 3.81, 3.76, 1H) 5.43 (s, 1H), 5.58 (dd, J = 1.79, 1.96,1H), 5.72 (d, J = 7.30,1H), 6.24 (t, J = 8.95, 1H), 7.36−8.11(m, 11H); ^{13}C NMR ($CDCl_3$) δ 14.4, 16.7, 20.6, 22.5, 22.7, 26.0, 27.1, 35.3, 36.3, 40.2, 42.5, 54.1, 54.9, 57.2, 72.6, 72.7, 75.5, 75.9, 76.8, 77.0, 77.3, 79.3, 82.1, 82.6, 126.7, 128.4, 128.7, 129.0, 129.3, 130.2, 133.7, 135.7, 137.2, 137.7, 167.1, 168.8, 172.2, 172.3, 214.9; APCI full MS m/z $[M + Na]^+$ 972.18.

Cytotoxicity Assay. Human tumor cells (A2780 ovarian carcinoma, A549 non-small lung carcinoma, and MCF-7 breast carcinoma) were plated at a density of 1000 cells/well in 96-well plates and allowed to attach overnight. These cell lines were maintained in RPMI-1640 medium supplemented with 5% fetal bovine serum and 5% Nu Serum and incubated at 37 °C. Taxanes were solubilized in DMSO and further diluted with RPMI-1640 medium. Triplicate wells were exposed to various treatments. The cell lines were analyzed for cytotoxicity using the microculture tetrazolium (MTT) procedure.[33]

Tubulin Polymerization Assay. The paclitaxel-facilitated tubulin polymerization assay was carried out with an assay kit from Cytoskeleton (BK006) according to the company's literature protocol. All samples and reagents were stored at −80 °C before use. Paclitaxel stocks were prepared in DMSO at 2 mM. The tubulin stock was prepared in a tubulin buffer containing 80 mM PIPES [piperazine-*N*,*N*′-bis(2-ethanesulfonic acid) sequisodium salt]; 2.0 mM $MgCl_2$, 0.5 mM EGTA, and 1.0 mM GTP, pH 6.9, at 10 mg/mL. To establish the assay, the tubulin stock was fast-thawed in a room-temperature water bath for 1 min and placed on ice. A polymerization buffer was prepared containing 80 mM PIPES at pH 6.9, 2 mM $MgCl_2$, 0.5 mM EGTA, 1 mM GTP, and 15% glycerol and kept on ice. Paclitaxel stocks were thawed to room temperature and diluted to 100 μM with the tubulin buffer. To start an assay, a microplate spectrophotometer (Spectra Max plus, Molecular Devices) was set to a constant temperature of 37 °C. A half-well 96-well plate was prewarmed for 30 min. A 10-μL portion of each of the diluted paclitaxel samples or control buffer was pipetted into wells of the microplate, and the plate was then incubated in the 37 °C spectrophotometer for 2 min. Immediately before use, 1 volume of the cold tubulin stock was mixed with 2 volumes of cold polymerization buffer. Then 100 μL of the mixture was swiftly pipetted into wells that contained paclitaxel or control buffer with care to avoid bubbles. Tubulin polymerization was monitored by measuring absorbance at 340 nm for 60 min at 1-min intervals.

X-ray Crystallographic Determination of Diastereomer Structures. Single crystals of **6** and **7** suitable for X-ray structure analysis were grown by slow evaporation at room temperature from acetonitrile and a mixture of acetonitrile and ether, respectively. The selected crystals were mounted on a Bruker D8 Advance diffractometer. Diffraction data were measured at 293(2) K using graphite-monochromated Mo Kα (0.71073 Å) radiation. The structures were solved by direct methods and refined by the full-matrix least-squares method on F_{obs}^2 by using the SHELXL-97 software package. All non-H atoms were anisotropically refined. The hydrogen atoms were located by calculation with respect to the related parent atoms. Complementary crystallographic data have been deposited with the CCDC as CCDC 241319 and CCDC 260830 for compounds **6** and **7**, respectively.

Conformational Analysis of the Diastereomers in Solution. NMR Spectroscopy. The concentration of both diastereomers for the NMR experiments was 41 mM in 80% DMSO-d_6/20% D_2O (v/v). All 2-D NMR spectra were acquired at 30 °C on a Varian Inova Unity 600 spectrometer. Interatomic NOE assignments were made from ROESY spectra recorded with a mixing time of 150 ms, respectively. The experimental data were acquired and processed using the Vnmr 6.1B program on a SUN SparcStation ultra 170 computer. The processed NMR data were visualized with the XEASY program. Peak-picking and peak-integration were achieved on a Silicon Graphics Indy R 5000 computer.

Restraint Determination. The distance limits were converted from the cross-peak intensities in the ROESY spectrum (mixing time 150 ms) by eq 1.

$$d_{ij} = d_{ref}\,(V_{ref}/V_{ij}) \quad (1)$$

The interproton distances can be obtained from the comparison between the intensities of cross-peak V_{ij} and the intensities of reference cross-peak V_{ref}. The two protons whose distance is 1.75 Å at position C6 were selected as the reference peak in the two Taxol derivatives. A total of 33 and 31 interproton distance constraints were obtained from **6** and **7**, respectively (see Supporting Information).

NAMFIS Analysis. Conformational searches were performed on each of the structures using MMFF and the GBSA/H_2O solvation model (MCMM, 25,000 steps for each diastereomer). The searches resulted in 3251 fully optimized unique conformations for **6**, with the global minimum found three times, and 2548 conformations for **7**, with the global minimum found six times. The full conformer dataset and the NMR NOE data were then integrated by the NAMFIS treatment to provide a "best fit" corresponding to six and four conformations with populations ranging from 49 to 5% and 45 to 4% for compound **6** and **7**, respectively.

Tubulin Docking. A local modification of the refined electron crystallographic complex[20] was made prior to docking. The M-loop was relocated from the experimental position to a region closer to the Taxol site. This allowed tubulin's Arg284 to play a more active role by forming a hydrogen bond with Taxol's C10 acetyl group. Without this modification, Glide (Schrödinger Inc.[45]) docks the Taxol structure in an inverted binding pose that directs the two C13 side chain phenyl rings out into solvent instead of deep within the hydrophobic pocket. Using the M-loop modified protein, however, Glide predicts Taxol with both the binding mode and T-Taxol conformation observed in the refined electron crystallographic complex. Therefore, each of the diastereomers was separately and flexibly Glide-docked into the locally modified complex. The best docking poses were chosen on the basis of the Emodel scoring function together with visualization to ensure reasonable binding modes.

Acknowledgment. Y.J. thanks Prof. Houming Wu (Shanghai Institute of Organic Chemistry) for 2-D NMR determination and is grateful to Prof. Haixia Lin (Department of Chemistry, Shanghai University) for encouragement and helpful discussion. We likewise are appreciative of Profs. Minqin Chen and Wengling Hong (Department of Chemistry, Fudan University) for the X-ray structure determinations. A.A.A. and J.P.S. are grateful to Prof. Dennis Liotta (Emory University) for encouragement and support.

Supporting Information Available: A detailed experimental section of NMR/NAMFIS analysis, four figures showing the

labeling schemes of hydrogen and carbon atoms, two tables of NOE distances for the two diastereomers, one full table of ^{13}C NMR data, and crystallographic information in CIF format. This material is available free of charge via the Internet at http://pubs.acs.org.

References

(1) Wani, M. C.; Taylar, H L.; Wall, M. E., Coggon, P.; McPhail, A. T. Plant Antitumor Agents. VI. The Isolation and Structure of Taxol, a Novel Antileukemic and Antitumor Agent from *Taxus brevifolia*. *J. Am. Chem. Soc.* **1971**, *93*, 2325−2327.

(2) (a) Tabata, H. Paclitaxel Production by Plant-Cell-Culture Technology. *Adv. Biochem. Eng. Biotechnol.* **2004**, *87*, 1−23. (b) Jennewein, S.; Croteau, R. Taxol: Biosynthesis, Molecular Genetics, and Biotechnological Applications. *Appl. Microbiol. Biotechnol.* **2001**, *57*, 13−9.

(3) Holmes, F. A.; Kudelka, A. P.; Kavanagh, J. J.; Huber, M, H.; Ajani, J. A.; Valero, V. In *Taxane Anticancer Agents*; Georg, G. I., Chen, T. T., Ojima, I.; Vyas, D. M., Eds.; ACS Symposium Series 583; American Chemistry Society; Washington, DC, 1995; p 31

(4) *Taxol: Science and Application*; Suffness, M., Ed.; CRC: Boca Raton, FL, 1995.

(5) Nicolaou, K. C.; Dai, W. M.; Guy, R, K. Chemistry and Biology of Taxol. *Angew. Chem., Int. Ed. Engl*. **1994**, *33*, 15−44.

(6) Kingston, D. G. I. Recent Advances in the Chemistry of Taxol. *J. Nat. Prod.* **2000**, *63*, 726−734.

(7) Schiff, P. B.; Fant, J.; Horwitz, S. B. Promotion of Microtubule Assembly in Vitro by Taxol. *Nature* **1979**, *277*, 665−667.

(8) Jimenez-Barbero, J.; Souto, A. A.; Abal, M.; Barasoain, I.; Evangelio, J. A.; Acuna, A. U.; Andreu, J. M.; Amat-Guerri, F. Effect of 2′-OH Acetylation on the Bioactivity and Conformation of 7-*O*-[*N*-(4′-Fluoresceincarbonyl)-L-alanyl]taxol. A NMR-fluorescence Microscopy Study. *Bioorg. Med. Chem.* **1998**, *6*, 1857−1863.

(9) Baker, J. K. Nuclear Overhauser Effect Spectroscopy (NOESY) and Dihedral Angle Measurements in the Determination of the Conformation of Taxol in Solution. *Spectrosc. Lett.* **1992**, *25*, 31−48.

(10) Hilton, B. D.; Chmurny, G. N.; Muschik, G. M. Taxol Quantitative Internuclear Proton−Proton Distances in $CDCl_3$ Solution from nOe Data: 2D NMR ROESY Buildup Rates at 500 MHz. *J. Nat. Prod.* **1992**, *55*, 1157−1161.

(11) Dubois, J.; Guénard, D.; Guéritte-Voegelein, F.; Guédira, N.; Potier, P.; Gillet, B. and Beloeil, J.-C. Conformation of Taxotere and Analogues Determined by NMR Spectroscopy and Molecular Modeling Studies. *Tetrahedron* **1993**, *49*, 6533−6544.

(12) Williams, H. J.; Scott, A. I.; Dieden, R. A.; Swindell, C. S.; Chirlian, L. E. Francl, M. M.; Heerding, J. M.; Krauss, N. E. NMR and Molecular Modeling Study of the Conformations of Taxol and of its Side Chain Methylester in Aqueous and Non-Aqueous Solution. *Tetrahedron* **1993**, *49*, 6545−6560.

(13) Ojima, I.; Kuduk, S. D.; Chakravarty, S.; Ourevitch, M.; Bégue, J.-P. A Novel Approach to the Study of Solution Structures and Dynamic Behavior of Paclitaxel and Docetaxel using Fluorine-Containing Analogues as Probes. *J. Am. Chem. Soc.* **1997**, *119*, 5519−5527.

(14) Vander Velde, D. G.; Georg, G. I.; Grunewald, G. L.; Gunn, C. W.; Mitscher, L. A. "Hydrophobic Collapse" of Taxol and Taxotere Solution Conformations in Mixtures of Water and Organic Solvent. *J. Am. Chem. Soc*. **1993**, *113*, 11650−11651.

(15) Paloma, L. G.; Guy, R. K.; Wrasidlo, W.; Nicolaou, K. C. Conformation of a Water-Soluble Derivative of Taxol in Water by 2D-NMR Spectroscopy. *Chem. Biol.* **1994**, *1*, 107−112.

(16) Ojima, I.; Chakravarty, S.; Inoue, T.; Lin, S.; He, L.; Horwitz, S. W.; Kuduk, S. D.; Danishefsky, S. J. A Common Pharmacophore for Cytotoxic Natural Products that Stabilize Microtubules. *Proc. Natl. Acad. Sci. U.S.A.* **1999**, *96*, 4256−4261.

(17) Snyder, J. P.; Nevins, N.; Cicero, D. O.; Jansen, J. The Conformations of Taxol in Chloroform. *J. Am. Chem. Soc.* **2000**, *122*, 724−725.

(18) Snyder, J. P.; Nettles, J. H.; Cornett, B.; Downing, K. H.; Nogales, E. The Binding Conformation of Taxol in β-Tubulin: A Model Based on Electron Crystallographic Density. *Proc. Natl. Acad. Sci. U.S.A.* **2001**, *98*, 5312−5316.

(19) Ganesh, T.; Guza, R. C.; Bane, S.; Ravindra, R.; Shanker, N.; Lakdawala, A. S.; Snyder, J. P.; Kingston, D. G. I. The Bioactive Taxol Conformation on β-Tubulin: Experimental Evidence from Highly Active Constrained Analogs. *Proc. Natl. Acad. Sci. U.S.A.* **2004**, *101*, 10006−10011.

(20) Nogales, E.; Wolf, S. G.; Downing, K. H. Structure of the $\alpha\beta$ Tubulin Dimer by Electron Crystallography. *Nature (London)* **1998**, *391*, 199−203.

(21) Querolle, O.; Dubois, J.; Thoret, S.; Roussi, F.; Guéritte, F.; Guénard, D. Synthesis of C2−C3′ N−Linked Macrocyclic Taxoids. Novel Docetaxel Analogs with High Tubulin Activity. *J. Med. Chem.* **2004**, *47*, 5937−5944.

(22) Johnson, S. A.; Alcaraz, A.; Snyder, J. P. T-Taxol and the Electron Crystallographic Density in β-Tubulin. *Org. Lett.* **2005**, *7*, 5549−5552.

(23) Jiang Y.; Lin H.-X.; Chen J.-M.; Chen M.-Q. Crystallographic Determination of Stereochemistry of Biologically Active 2″,3″-Dibromo-7-*epi*-10-deacetylcephalomannine. *Bioorg. Med. Chem. Lett.* **2005**, *15*, 839−842.

(24) Cody, V.; Murray-Rust, P. Iodine···X (O, N, S) Intermolecular Contacts: Models of Thyroid Hormone−Protein Binding Interactions Using Information from the Cambridge Crystallographic Data Files. *J. Mol. Struct.* **1984**, *112*, 189−199.

(25) Ouvrard, C.; Le Questel, J. Y.; Berthelot, M.; Laurence, C. Halogen-Bond geometry: A Crystallographic Database Investigation of Dihalogen Complexes. *Acta Crystallogr. B* **2003**, *59*, 512−526.

(26) Lommerse, J. P. M.; Stone, A. J.; Taylor, R.; Allen, F. H. The Nature and Geometry of Intermolecular Interactions between Halogens and Oxygen and Nitrogen. *J. Am. Chem. Soc.* **1996**, *118*, 3108−3116.

(27) Corradi, E.; Meille, S. V.; Messina, M. T.; Metrangolo, P., Resnati, G. Halogen Bonding versus Hydrogen Bonding in Driving Self-Assembly Processes. *Angew. Chem., Int. Ed.* **2000**, *112*, 1852−1856.

(28) Lommerse, J. P. M.; Price, S. L.; Taylor, R. Hydrogen Bonds of Carbonyl, Ether and Ester Oxygen Atom and Alkanol Hydroxyl Groups. *J. Comput. Chem.* **1997**, *18*, 757−774.

(29) Auffinger, P.; Hays, F. A.; Westhof, E.; Ho, P. S. Halogen Bonds in Biological Molecules. *Proc. Natl. Acad. Sci. U.S.A.* **2004**, *101*, 16789−16794.

(30) (a) Irving, R.; George, E. K. The Halogenation of Ethylenes. *J. Am. Chem. Soc*. **1937**, *59*, 947−748. (b) John McMurry, *Organic Chemistry*; 6th ed.; Brooks/Cole: Belmont, CA, 2004; pp 208−210.

(31) Rimoldi, J. M.; Molinero, A. A.; Chordia, M. D.; Gharpure, M. M.; Kingston, D. G. I. An Improved Method for the Separation of Paclitaxel and Cephalomannine. *J. Nat. Prod.* **1996**, *59*, 167−168.

(32) Pandey, R. C.; Yankov, L. K.; Poulev, A.; Nair, R.; Caccamese, S. Synthesis and Separation of Potential Anticancer Active Dihalocephalomannine Diastereomers from Extracts of *Taxus yunnanensis*. *J. Nat. Prod.* **1998**, *61*, 57−63.

(33) Mosmann, T. Rapid Colorimetric Assay for Cellular Growth and Survival: Application to Proliferation and Cytotoxicity Assays. *J. Immunol. Methods.* **1983**, *65*, 55−63; cf. http://www.protocol-online.org/prot/Cell_Biology/Cell_Growth_Cytotoxicity/MTT_Cell_Proliferation_Assay/.

(34) Mastropaolo, D.; Camerman. A.; Luo, Y.; Brayer, G. D.; Camerman, N. Crystal and Molecular Structure of Paclitaxel (Taxol). *Proc. Natl Acad. Sci. U.S.A.* **1995**, *92*, 6920−6924.

(35) Gao, Q.; Williams, L. P. The Hydrophobic Collapse Conformation of Paclitaxel Has Been Observed in a Non-Aqueous Environment: Crystal Structure of 10-Deacetyl-7-epitaxol. *Tetrahedron*. **1996**, *52*, 2291−2300.

(36) Guéritte-Voegelein, F.; Guénard, D.; Mangatal, L.; Potier, P.; Guilhem, J.; Cesario, M.; Pascard, C. Structure of a Synthetic Taxol Precursor: *N-tert*-Butoxycarbonyl-10-deacetyl-*N*-debenzoyltaxol. *Acta Crystallogr., Sect. C: Cryst. Struct. Commun.* **1990**, *46*, 781−782.

(37) Gibson, F. S.; Wei, J.; Vemishetti, P.; Gao, Q.; Dillon, J. L. Synthesis, Utility, and X-ray Crystal Structure of Novel Complexes of Baccatin III with Imidazole and 2-Propanol. *Org. Lett.* **2000**, *2*, 3269−3271.

(38) (a) Jiménez-Barbero, J.; Amat-Guerri, F.; Snyder, J. P. The Solid State, Solution and Tubulin-Bound Conformations of Agents That Promote Microtubule Stabilization. *Curr. Med. Chem.*−Anti-Cancer Agents. **2002**, *2*, 91−122. (b) Zefirova, O. N.; Nurieva, E. V.; Ryzhov, A. N.; Zyk, N. V.; Zefirov, N. S. Taxol: Synthesis, Bioactive Conformations, and Structure−Activity Relationships in Its Analogs. *Russ. J. Org. Chem.* **2005**, *41*, 315−351.

(39) Kingston, D. G. I.; Bane, S.; Snyder, J. P. The Taxol Pharmacophore and the T-Taxol Bridging Principle. *Cell Cycle* **2005**, *4*, 279−289.

(40) Dumas, J. M.; Geron, C.; Kribii, A. R.; Lakraimi, M. Structural and Thermodynamic Studies of Interactions between Chlorinated and Brominated Derivatives of Methane and Tertiary Amides. *Can. J. Chem.* **1984**, *62*, 2634−2640.

(41) Bondi, A. van der Waals Volumes and Radii. *J. Phys. Chem.* **1964**, *68*, 441−451.

(42) Nevins, N.; Cicero, Daniel.; Snyder J. P. A Test of the Single-Conformation Hypothesis in the Analysis of NMR Data for Small Polar Molecules: A Force Field Comparison. *J. Org. Chem.* **1999**, *64*, 3979−3986.

(43) Cicero, D. O.; Barbato, G.; Bazzo, R. NMR Analysis of Molecular Flexibility in Solution: A New Method for the Study of Complex Distributions of Rapidly Exchanging Conformations. Application to a 13-Residue Peptide with an 8-Residue Loop. *J. Am. Chem. Soc.* **1995**, *117*, 1027−1033.

(44) Lakdawala, A.; Wang, M.; Nevins, N.; Liotta, D. C.; Rusinska-Roszak, D.; Lozynski, M. C.; Snyder, J. P. Calculated Conformer Energies for Organic Molecules with Multiple Polar Functionalities are Method Dependent: Taxol Case Study. *BMC Chem. Biol.* **2001**, *1*, 2; http://www.biomedcentral.com/1472−6769/1/2.

(45) (a) Friesner, R. A.; Banks, J. L.; Murphy, R. B.; Halgren, T. A.; Klicic, J. J.; Mainz, D. T.; Repasky, M. P.; Knoll, E. H.; Shaw, D. E.; Shelley, M.; Perry, J. K.; Sander, L. C.; Shenkin, P. S. Glide: A New Approach for Rapid, Accurate Docking and Scoring. 1. Method and Assessment of Docking Accuracy. *J. Med. Chem.* **2004**, *47*, 1739−1749. (b) Halgren, T. A.; Murphy, R. B.; Friesner, R. A.; Beard, H. S.; Frye, L. L.; Pollard, W. T.; Banks, J. L. Glide: A New Approach for Rapid, Accurate Docking and Scoring. 2. Enrichment Factors in Database Screening. *J. Med. Chem.* **2004**, *47*, 1750−1759.

(46) Nettles, J. H.; Li, H.; Cornett, B.; Krahn, J. M.; Snyder J. P.; Downing K. H. The Binding Mode of Epothilone A on α, *β*-Tubulin by Electron Crystallography. *Science* **2004**, *305*, 866−869.

(47) Hari, M.; Loganzo, F.; Annable, T.; Tan, X.; Musto, S.; Morilla, D. B.; Nettles, J. H.; Snyder, J. P.; GreenbergerL. M. Paclitaxel Resistant Cells have a Mutation in the Paclitaxel-Binding Region of *β*-Tubulin (Asp26Glu) and Less Stable Microtubules. *Mol. Can. Therapeutics* **2006**, in press.

(48) Alcaraz, A. A.; Mehta, A. K.; Johnson, S. A.; Snyder, J. P. The T-Taxol Conformation. Submitted.

JM0509243